Development of a Highly Selective, Sensitive, and Fast Response Upconversion Luminescent Platform for Hydrogen Sulfide Detection

Juanjuan Peng, Chai Lean Teoh, Xiao Zeng, Animesh Samanta, Lu Wang, Wang Xu, Dongdong Su, Lin Yuan, Xiaogang Liu, and Young-Tae Chang**

Hydrogen sulfide (H_2S) has been recognized as one of most important gaseous signaling molecules mediated by a variety of physiological and pathological processes. Yet, its functions remain largely elusive due to the lack of potent monitoring methods. Hereby this issue is addressed with a powerful new platform—dye-assembled upconversion nanoparticles (UCNPs). A series of chromophores with different absorption bands and fast responses towards H_2S is combined with UCNPs and results in a library of H_2S sensors with responsive emission signals ranging from the visible to the near-infrared (NIR) region. These nanoprobes demonstrate highly selective and rapid responses to H_2S in vitro and in cells. Furthermore, H_2S levels in blood can be detected using the developed nanoprobes. Hence the reported H_2S sensing platform can serve as a powerful diagnostic tool to research H_2S functions and to investigate H_2S-related diseases.

1. Introduction

Hydrogen sulfide (H_2S) is traditionally considered as a toxic gas with the stink of rotten eggs. However, the roles of H_2S in living organisms have received more and more attention in recent years, especially after this molecule was recognized as the third endogenous gas transmitter functioning in a variety of internal systems, along with nitric oxide (NO) and carbon monoxide (CO).[1] Studies have shown that H_2S have an effect on the cardiovascular system,[2] regulates cell growth,[3] relaxes blood vessels,[4] and modulates neuronal excitability.[5] However, abnormal concentration of H_2S is also related to many diseases, such as Down syndrome,[6] Alzheimer's diseases,[7] and liver cirrhosis.[8] These findings highlight importance of H_2S homeostasis, yet the lack of powerful monitoring methods that could offer both spatial and temporal precision has hampered the investigation of H_2S functions. Therefore, the rapid, facile, and reliable detection and monitoring of H_2S with high sensitivity and selectivity in biological systems would be highly desirable and beneficial.

Fluorescence technique, especially small molecule fluorescent sensors, has been employed in the noninvasive detection of H_2S owing to its sensitivity and adaptability.[9] Despite the increasing effort in the preparation and study of suitable fluorescent H_2S sensors, there are still several challenges are present, 1) thiol containing biomolecules can interfere with H_2S concentration reading due to the non-specificity suffered from current luminescence probes, 2) the signal-to-noise ratio can also be compromised by the autofluorescence generated by proteins and peptides within samples, 3) majority of the fluorescent sensors require substantial incubation period to fully fluoresce under mild physiological conditions, and 4) due to the intrinsic chemical instability of fluorophores at excited state, fluorescent sensors suffer from serious photobleaching and decomposition. Therefore alternative monitoring approaches are actively being pursued combing with the small molecule fluorescent sensors together.

With the unique ability to convert long-wavelength low energy light to short-wavelength high energy light, lanthanide-doped upconversion nanoparticles (UCNPs) have been

Dr. J. Peng, Dr. C. L. Teoh, Dr. A. Samanta, Dr. D. Su, Prof. Y.-T. Chang
Singapore Bioimaging Consortium
Agency for Science, Technology and Research (A* STAR)
138667, Singapore
X. Zeng, L. Wang, Dr. W. Xu, Prof. L. Yuan, Prof. X. Liu, Prof. Y.-T. Chang
Department of Chemistry
National University of Singapore
117543, Singapore
E-mail: chmcyt@nus.edu.sg

Prof. L. Yuan
State Key Laboratory of Chemo/Biosensing and Chemometrics
College of Chemistry and Chemical Engineering
Hunan University
Changsha 410082, Hunan, P. R. China
E-mail: lyuan@hnu.edu.cn

Prof. X. Liu
Institute of Materials Research and Engineering
Agency for Science, Technology and Research (A* STAR)
117602, Singapore

Prof. X. Liu
Center for Functional Materials
NUS (Suzhou) Research Institute
Suzhou, Jiangsu 215123, P. R. China

DOI: 10.1002/adfm.201503715

considered as a new generation of promising luminescent probes. They possess an abundant of intriguing characteristics,[10] such as a large anti-Stokes shift of up to several hundred nanometers, high photostability, no blinking, high penetration depth, and no autofluorescence from biosamples. On the other hand, chromophores with specific recognition sites have been widely used for highly selective sensing application. Therefore, it is reasonable to assume that the hybrid system of UCNPs and chromophores has the outstanding recognition properties of chromophores and remarkable imaging capacity from UCNPs. To date, several UCNPs-based fluorescence resonance energy transfer (FRET) nanosystems have been developed for detection of important biological species and toxin, such as DNA, O_2, CN^-, Hg^{2+}, and Zn^{2+},[11] in which the energy-transfer process is utilized to modulate the upconversion luminescence (UCL) intensity. Thus the use of UCL generated by UCNPs to monitor H_2S may be a feasible strategy, the reported probes[9i,j] can be hardly used to monitoring H_2S levels in vivo because of the narrow response range, slow response time, and short emission wavelength. Therefore, it is of importance to developed H_2S detection probes with fast response and broad liner range.

In this work, three H_2S-responsive dyes with high sensitivity, selectivity, and fast response were synthesized (compound **1**, **2**, and **3**[12] as sulfide sensing probes, whereas two kinds of UCNPs including $NaYF_4$:Yb/Er/Tm (20/1.6/0.4 mol%) with green UCL and $NaYF_4$:Yb/Mn/Er (20/30/2 mol%) with pure red UCL were synthesized as energy donors. The absolute quantum yield of the $NaYF_4$:Yb/Er/Tm and $NaYF_4$:Yb/Mn/Er was, respectively, measured to be 0.021% and 0.013% on a Edinburgh FLS980 spectrometer equipped with an integrating sphere by reported method.[13] The compounds were loaded to the surface of UCNPs through electrostatic interactions. The dyes have been designed to absorb at the same wavelengths as the emission of UCNPs, hence energy transfer would occur from the UCNPs (donor) to the chromophores (acceptor), leading to luminescence quenching of upconversion emission. As sulfide species bleaches the chromophore in a specific and efficient manner, the restored upconversion emission can serve as a ratiometic indicator in reporting not only the presence but also the concentration of existing H_2S in vitro, in cells, and blood serum.

2. Results and Discussion

2.1. Design Principle of the UCL Nanosensor for H_2S

Scheme 1 shows the design strategy of the UCL probes for H_2S, which based on the energy-transfer (ET) processes between UCNPs and the loaded chromophores. Two kinds of UCNPs, $NaYF_4$:Yb/Er/Tm (20/1.6/0.4 mol%) with green UCL and $NaYF_4$:Yb/Mn/Er (20/30/2 mol%) with red UCL were respectively used as a energy donor. Three H_2S-responsive compounds **1**, **2**, or **3** were employed as acceptors and selectively assembled on the surface of the two UCNPs to construct four kinds of dye-UCNP nanoprobes, which were denoted as **1**-PAA-$NaYF_4$:Yb/Er/Tm, **2**-PAA-$NaYF_4$:Yb/Er/Tm, **3**-PAA-$NaYF_4$:Yb/Er/Tm, and **3**-PAA-$NaYF_4$:Yb/Mn/Er, respectively. Without modification of compounds, the UCNPs gave rise to

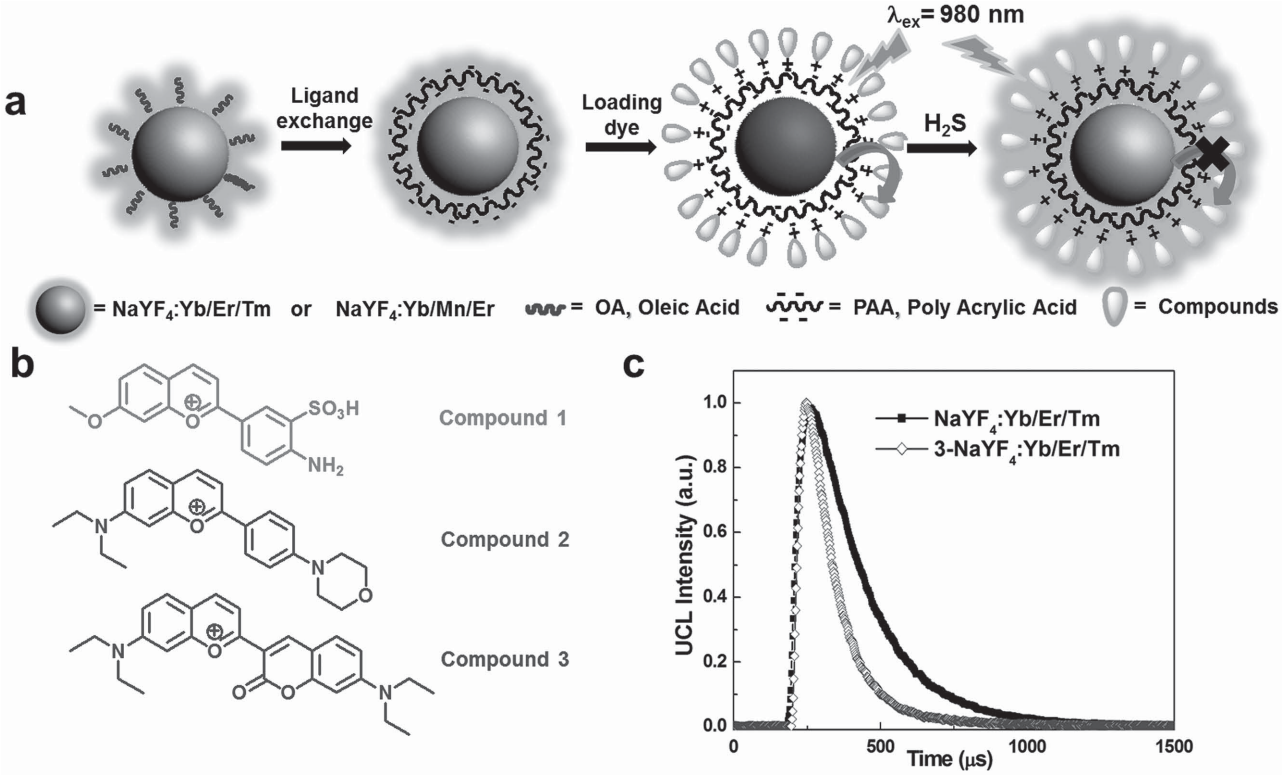

Scheme 1. a) Schematic illustration showing the synthesis of chromophore-assembled UCNPs and their response to H_2S. b) Molecular structure of compounds **1**, **2**, and **3**. c) Life-time of $NaYF_4$:Yb/Er/Tm (λ_{em} = 650 nm) before and after modification of compound **3**.

green or red emissions originating from the $^4S_{2/3} \rightarrow {}^4I_{15/2}$ or $^4S_{9/2} \rightarrow {}^4I_{15/2}$ transition of Er^{3+} under the excitation of a 980 nm laser. However, after attachment with the compounds, the UCL signals were quenched by the ET between the UCNPs and the dyes. When H_2S was present in the prepared nanoprobes, the absorption of compound **1**, **2**, and **3** was strongly suppressed due to the disruption of the conjugation structure by H_2S (**Figure 1**). Since the emission between UCNPs and absorption bands of attached compounds no longer overlapped, the green or red emissions of UCNPs were thus recovered. In addition, the doped Tm^{3+} into $NaYF_4$:Yb/Er/Tm introduced UCL signals at 800 nm as an internal reference, which can be used for ratiometric detection of H_2S.

2.2. Synthesis and Characterization of 1, 2, 3-UCNPs

In the present study, in order to obtain effective UCL, two kinds of nanoparticles, $NaYF_4$:Yb/Er/Tm with an average diameter ≈13 nm and $NaYF_4$:Yb/Mn/Er with an average diameter ≈12 nm were prepared according to the literatures (**Figure 2**a,d; Figures S1 and S2, Supporting Information), respectively.[14] The morphology difference between sphere $NaYF_4$:Yb/Er/Tm and square $NaYF_4$:Yb/Mn/Er can be clearly observed from the TEM images. It should be noted that doping Mn^{2+} ion into $NaYF_4$ induced the hexagonal-to-cubic phase transformation (Figure 2b,e). On the other hand, the introduction of Mn^{2+} ions into $NaYF_4$:Yb/Er led to a brilliant red emission (650 nm) compared to the green color of $NaYF_4$:Yb/Er/Tm without Mn^{2+} doping (Figure 2c,f). It is worth noting that both the external excitation and the red emission (980 nm/650 nm) are within the "optical window" of biological tissues, which enables deep tissue imaging and blood testing. As shown in Scheme 1, to integrate UCNPs and the compounds together into one nanosystem, the oleic acid (OA) ligands on the surface of UCNPs were first replaced by negatively charged hydrophilic polyacrylic acid (PAA). During the ligand-exchange process, the size and morphology of nanocrystals did not change as revealed from TEM images (Figure S3 and S4, Supporting Information). Subsequently, positively charged compounds **1**, **2**, and **3** were assembled onto the UCNPs surface through electrostatic attraction. The change of zeta potential of bare UCNP, PAA-UCNPs, and UCNPs modification with the compounds was studied. The zeta potential of bare $NaYF_4$:Yb/Er/Tm and PAA-$NaYF_4$:Yb/Er/Tm were +56.8 mV and −42.4 mV, respectively. After the PAA-$NaYF_4$:Yb/Er/Tm were modified with compounds **1**, **2**, and **3**, the zeta potential changed to +14.0, +13.9, and +1.87 mV (Figure S5–S9, Supporting Information). The zeta potential of bare $NaYF_4$:Yb/Mn/Er, PAA-$NaYF_4$:Yb/Mn/Er, and **3**-$NaYF_4$:Yb/Mn/Er were +47.5, −31.7, and −2.82 mV, respectively (Figures S10–S12, Supporting Information). In order to confirm the energy transfer between UCNPs and dyes, the lifetime of green and red emission of UCNPs in presence of compounds **1**, **2**, and **3** was investigated. The lifetime of $NaYF_4$:Yb/Er/Tm at 541 nm decreased from 93.3 to 82.2 μs or 70.9 μs after modification with compound **1** or **2**, respectively

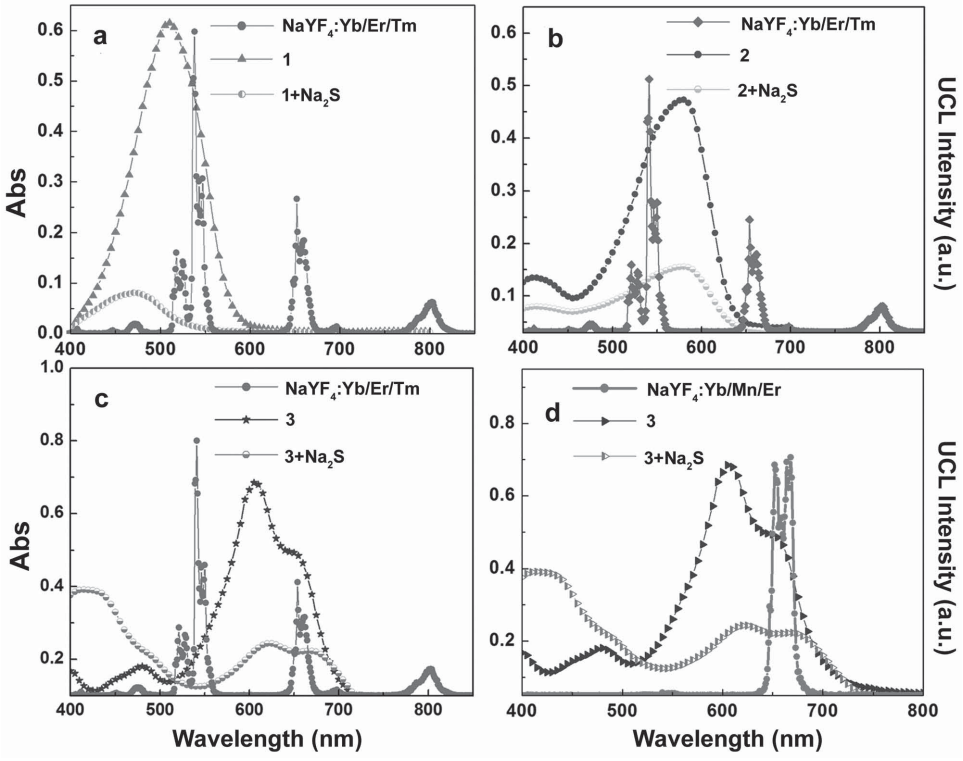

Figure 1. UV–Vis absorption spectra of a) compound **1** (0.15×10^{-3} M), b) compound **2**, (0.056×10^{-3} M), c,d) compound **3** (0.3×10^{-3} M) in the absence and presence of Na_2S (0.15×10^{-3} M), and the UCL spectra of $NaYF_4$:Yb/Er/Tm (line with filled circles in (a,c), line with diamonds in (b)) and $NaYF_4$:Yb/Er/Mn (line with filled circles in (d)) under 980 nm excitation.

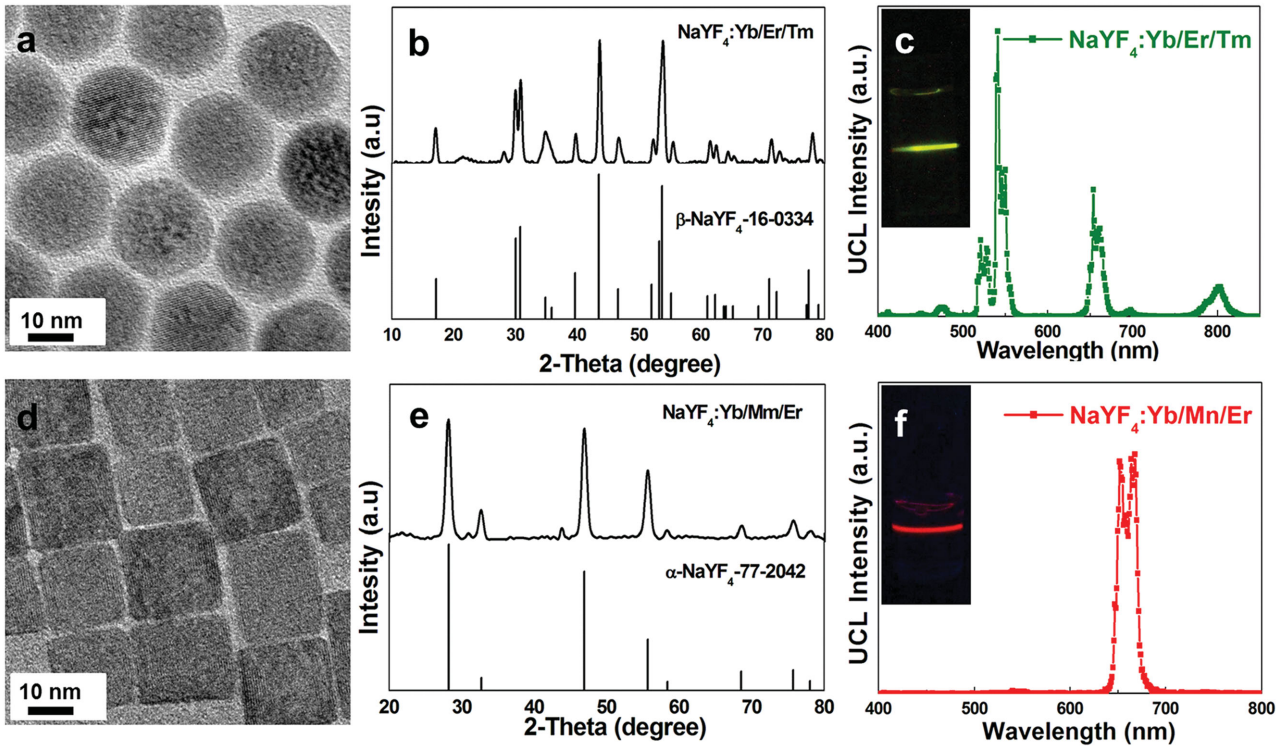

Figure 2. TEM image of a) OA-$NaYF_4$:Yb/Er/Tm and d) OA-$NaYF_4$:Yb/Er/Mn. b) XRD patterns of OA-$NaYF_4$:Yb/Er/Tm and the standard pattern of pure hexagonal $NaYF_4$ (JCPDS card No.16-0334). e) XRD patterns of OA-$NaYF_4$:Yb/Er/Mn and the standard pattern of pure cubic $NaYF_4$ (JCPDS card No.77-2042). Upconversion luminescent emission (UCL) spectrum of the c) $NaYF_4$:Yb/Er/Tm and f) $NaYF_4$:Yb/Er/Mn excited with a CW 980 nm laser. Inset: the luminescence photograph of the UCNPs appear green and red color, respectively, under CW excitation at 980 nm.

(Figures S13, S14, Supporting Information), and the lifetime of $NaYF_4$:Yb/Er/Tm at 650 nm changed from 182.6 μs to 171.6 μs, 166.1 μs or 136.7 μs after modified with compounds **1**, **2**, or **3**, respectively (Figures S15, S16, Supporting Information, Scheme 1c). Comparing the lifetime decay of the green and red emission after modification with compounds **1**, **2**, and **3**, it can be concluded that the lifetime of the green emission decreased more significantly than the red emission, because the absorption of compounds **1** and **2** matched better with the green emission while the compound **3** matched with the red emission of UCNPs. All of the results proved the compounds were successfully modified to the surface of UCNPs and the energy transfer between the UCNPs and the compounds. The efficiency of the FRET processes were calculated through the following formula:[15]

$$E = 1 - \frac{\tau_{DA}}{\tau_D} \quad (1)$$

where τ_D is the lifetime of donor and τ_{DA} is the lifetime of donor in the present of acceptor. According to the lifetime change of $NaYF_4$:Yb/Er/Tm at 541 nm before and after modification with compounds **1**, **2**, the FRET efficiency between $NaYF_4$:Yb/Er/Tm and compounds **1**, **2** are 11.8% and 24.0%, respectively. After calculating the lifetime of $NaYF_4$:Yb/Er/Tm at 650 nm before and after modification with compound **3**, we concluded that the FRET efficiency between $NaYF_4$:Yb/Er/Tm and compound **3** is 25.1%. The decrease of the average lifetime indicates that quenching of UCL occurs not only through the Förster resonance energy transfer but also through reabsorption. The absorption spectroscopy results reveal that the amount of compounds **1**, 2, and **3** on the surface of the UCNPs was 0.49×10^{-3}, 0.48×10^{-3} and 0.52×10^{-3} M, which was ≈6.48, 6.96, and 8.04 wt% of the **1**-PAA-$NaYF_4$:Yb/Er/Tm, **2**-PAA-$NaYF_4$:Yb/Er/Tm, and **3**-PAA-$NaYF_4$:Yb/Mn/Er (Figure S17–S19, Supporting Information). To prove the stability of **1**-PAA-$NaYF_4$:Yb/Er/Tm, **2**-PAA-$NaYF_4$:Yb/Er/Tm, **3**-PAA-$NaYF_4$:Yb/Er/Tm :Yb/Er/Tm, and **3**-PAA-$NaYF_4$:Yb/Mn/Er in biological environments, the as-prepared nanoprobes were dispersed in different media, such as water, PBS, HEPES. It was found that the UCL signals remained essentially constant, clearly suggesting that the developed nanoprobes were sufficient stable for sensing and bioimaging experiments.

2.3. H_2S Sensing Capabilities by 1, 2, 3-UCNPs

The sensing performance of developed nanoprobes was investigated through UV–vis absorption and photoluminescence titrations. Different concentration of Na_2S was added into the aqueous solution containing as-prepared nanoprobes. As shown in **Figure 3**a, upon addition of Na_2S to the solution of **1**-PAA-$NaYF_4$:Yb/Er/Tm, a significant increase in the UCL intensity at 541 nm could be observed due to the Na_2S-induced significant hypochromicity at 548 nm, indicating the nucleophilic addition reaction between compound **1** and Na_2S

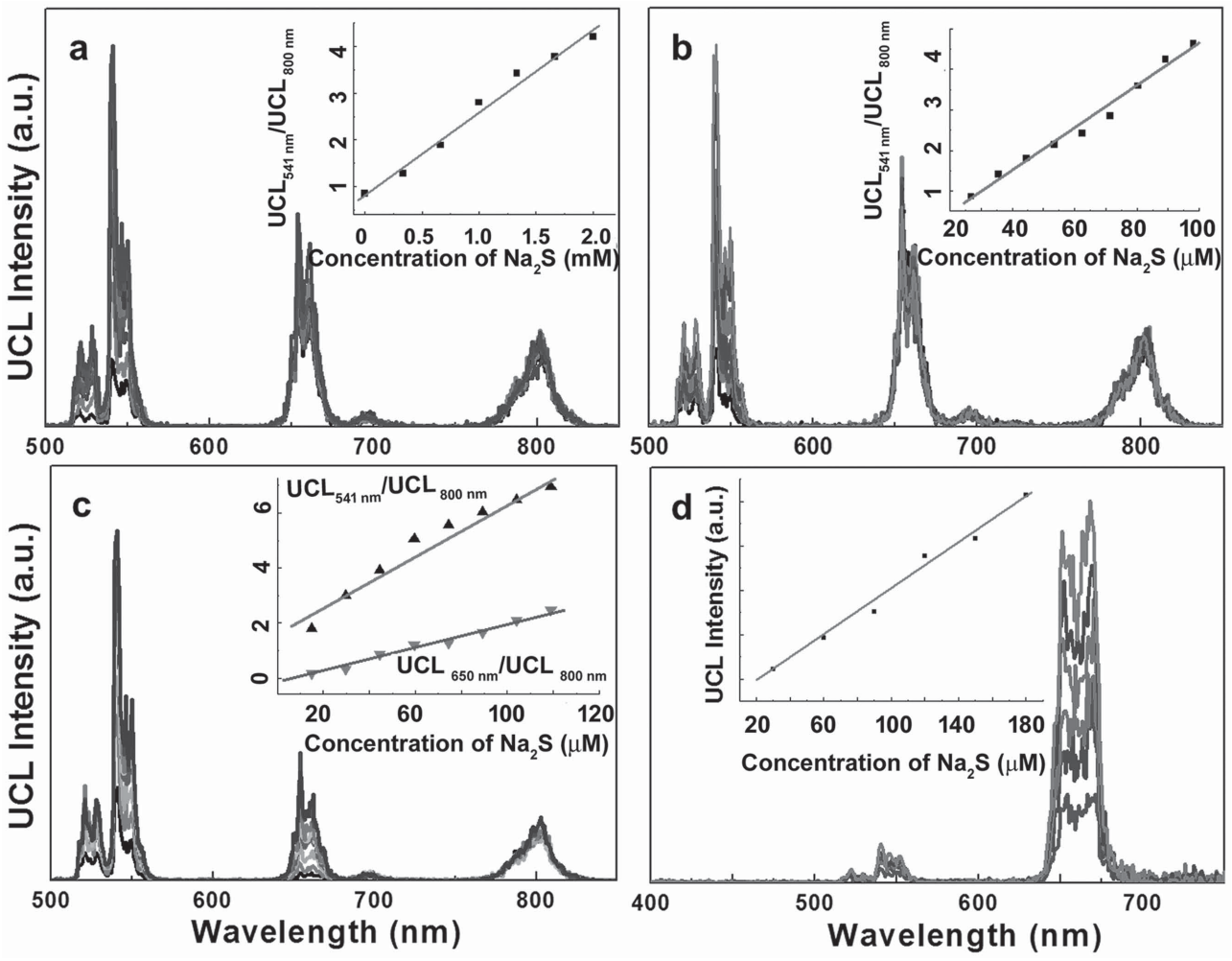

Figure 3. UCL spectra of a) **1**-PAA-$NaYF_4$:Yb/Er/Tm, b) **2**-PAA-$NaYF_4$:Yb/Er/Tm, c) **3**-PAA-$NaYF_4$:Yb/Er/Tm and d) **3**-PAA-$NaYF_4$:Yb/Er/Mn (0.25 mg mL^{-1}) upon gradual addition of Na_2S. Inset in (a,b): The UCL emission ratio intensity at 541 and 800 nm ($UCL_{541\ nm}/UCL_{800\ nm}$). Inset in (c): UCL emission ratio intensity at 541 and 800 nm ($UCL_{541\ nm}/UCL_{800\ nm}$) and at 650 and 800 nm ($UCL_{650\ nm}/UCL_{800\ nm}$) as a function of the Na_2S concentration. Inset in (d): The UCL emission intensity at 650 nm as a function of the Na_2S concentration.

(Figure S20, Supporting Information). The same phenomenon can be observed about the compound **2** modified $NaYF_4$:Yb/Er/Tm (Figure 3b; and Figure S21, Supporting Information), and the sensitivity of **2**-PAA-$NaYF_4$:Yb/Er/Tm is higher than the **1**-PAA-$NaYF_4$:Yb/Er/Tm. The ratio $I_{541\ nm}/I_{800\ nm}$ was used to reflect the concentration of Na_2S, which shows a linear increase in the range of 0–100 × 10^{-6} M Na_2S. It should be noted that both the UCL intensity at 541 nm and 650 nm are significant increased (Figure 3c) because compound **3** has a broad absorption band between 500 and 700 nm and quenches the UCL at 541 nm and 650 nm (Figure S22, Supporting Information) simultaneously after loading to the surface of $NaYF_4$:Yb/Er/Tm. Also, both ratio $I_{541\ nm}/I_{800\ nm}$ and $I_{650\ nm}/I_{800\ nm}$ show a linear increase in the range of 0–115 × 10^{-6} M Na_2S (Figure 3c, inset). Based on this, we synthesized $NaYF_4$:Yb/Mn/Er with pure red color and combined it with compound **3** to get the NIR probe. And till now, the developed UCNPs based probes for H_2S detection are all UV–Vis probes. The UCL intensity at 650 nm was enhanced with the increasing of concentration of Na_2S (Figure 3d and inset). Surprisingly, we found that the interaction between nanoprobes and sulfide is finished within 5 s (movie in Supporting Information), enabling rapid detection and real-time monitoring of sulfide species. Meanwhile, the mechanism and the products of compounds **1**, **2**, and **3** reacting with Na_2S were confirmed by reversed-phase HPLC chromatograms with absorption detection at 500 nm (Figures S23, S24, Supporting Information). Before reaction, the compound **1** shows only one peak at 4.00 min, whereas after reacting with Na_2S, a new peak at 5.33 min appears with the mass peak m/e 364, representing a negatively charged species of $[\mathbf{1}\text{-HS}]^-$. The similar phenomena can be observed after reaction of compounds **2** and **3** with Na_2S (Figures S25–S28, Supporting Information). New peaks at 7.76 or 7.96 min appear with the mass peak m/e 397.2 or 451.3, respectively, representing a negatively charged species of $[\mathbf{2}\text{-HS}]^-$ or $[\mathbf{3}\text{-HS}]^-$.

To further investigate the selectivity of the developed nanoprobes, we examined the changes in UCL spectra of **1**-PAA-$NaYF_4$:Yb/Er/Tm, **2**-PAA-$NaYF_4$:Yb/Er/Tm, and **3**-PAA-$NaYF_4$:Yb/Er/Tm incubated with various reactive species for

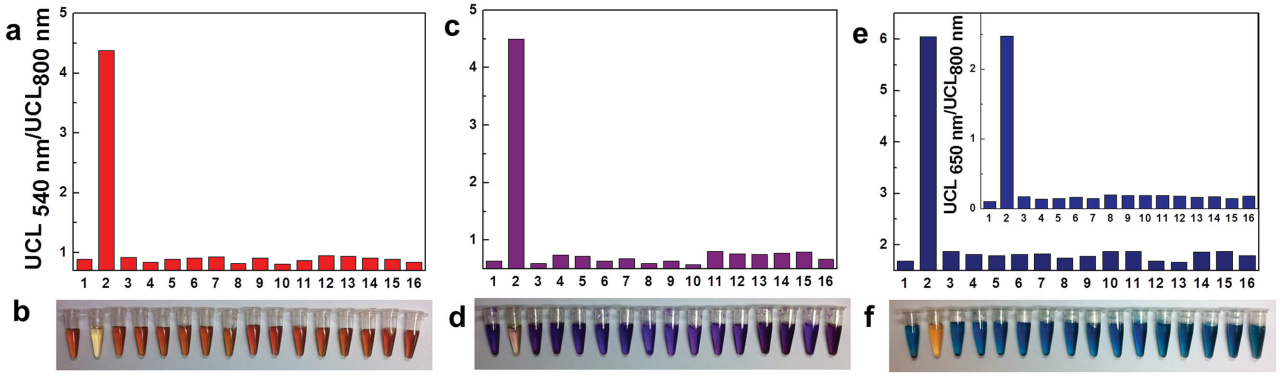

Figure 4. a,c,e) UCL changes in $UCL_{541\ nm}/UCL_{800\ nm}$ and b,d,f) $UCL_{650\ nm}/UCL_{800\ nm}$, the color changes of **1**-$NaYF_4$:Yb/Er/Tm, **2**-$NaYF_4$:Yb/Er/Tm, and **3**-$NaYF_4$:Yb/Er/Tm (0.25 mg mL^{-1}) upon addition of various ROS and ions in the aqueous solution. 1) blank, 2) H_2S (0.2×10^{-3} M), 3–5) Cys, GHS, and Hcy (10×10^{-3} M), 6,7) H_2O_2, BuOOH (6×10^{-3} M), 8,9) sulfur-containing inorganic ions ($S_2O_3^{2-}$, SO_4^{2-}, 8×10^{-3} M) and 10–16) different ions (Zn^{2+}, Ba^{2+},Ca^{2+}, Fe^{3+}, K^+, Na^+, Mn^{2+}, 10×10^{-3} M).

5 min, including ROS and common inorganic anions. No significant changes in ratiometric UCL emission were observed when the systems were treated with ROS (H_2O_2, *t*-BuOOH), sulfur-containing inorganic ions ($S_2O_3^{2-}$, SO_4^{2-}) and different biological metal ions (K^+, Na^+, Mn^{2+}, Ca^{2+}, Fe^{3+}) (**Figure 4**; and Figure S29, Supporting Information). Notably, biological thiols (cysteine, glutathione, and homocysteine) did not induce UCL response of the as-prepared luminescence probes, even though cysteine, glutathione, and homocysteine are ubiquitous in living systems and have very similar nucleophilicity as H_2S. All of the results indicate the good selectivity of our developed probes. Therefore, **1**-PAA-$NaYF_4$:Yb/Er/Tm, **2**-PAA-$NaYF_4$:Yb/Er/Tm, and **3**-PAA-$NaYF_4$:Yb/Er/Tm can potentially act as highly selective UCL probes for H_2S in vivo without the interference from other biologically relevant analytes.

2.4. Monitoring of H_2S in Live Cells

To demonstrate the potential application of as-prepared probes for bioimaging, the cytotoxicity of **1**-PAA-$NaYF_4$:Yb/Er/Tm, **2**-PAA-$NaYF_4$:Yb/Er/Tm, **3**-PAA-$NaYF_4$:Yb/Er/Tm, and **3**-$NaYF_4$:Yb/Er/Mn were first evaluated on the basis of the reduction activity of methyl thiazolyl tetrazolium (MTT) assay. In our study, HeLa cell line (HeLa: cervical carcinoma) was selected. The cell viabilities are all higher than 95% with the exposure of 600 μg mL^{-1} dose for 24 h (Figure S30–S33, Supporting Information), suggesting that the nanoprobes have good biocompatibility. Because **2**-PAA-$NaYF_4$:Yb/Er/Tm shows the best sensitivity among the three probes and **3**-$NaYF_4$:Yb/Er/Mn is a NIR probe, the two are selected and used for monitoring H_2S in live cells. The cells were incubated with the nanoparticles (250 μg mL^{-1} for 1 h) and analyzed under an optical fluorescence microscope equipped with a 980 nm laser. As shown in **Figure 5**, cells incubated with **2**-PAA-$NaYF_4$:Yb/Er/Tm or **3**-$NaYF_4$:Yb/Mn/Er at 37 °C for 1 h showed very dim green or red UCL emission (Figure 5b,f). After the cells were supplemented with Na_2S (100×10^{-6} M) in the growth medium for 0.5 h at 37 °C, they were imaged under the same condition, and a significant enhancement of green UCL emission and red UCL were observed in the intracellular region (Figure 5d,h). By monitoring variation of the UCL intensity from the cells in the presence or absence of Na_2S, a semiquantitative detection could be achieved (Figure 5i,j). The UCL spectra of cell imaging in the presence or absence of Na_2S also proved that the as-prepared probes were suitable for monitoring H_2S in living cells (Figure S34, Supporting Information). It should be noted that by quantifying the UCL signal in regions 1 and 2 in Figure 5d, an excellent signal-to-noise ratio with no autofluorescence (counts ≈0) and extremely intense UCL (counts ≈40, Figure S5, Supporting Information) were obtained. Such a high signal-to-noise ratio could be hardly obtained by conversional fluorescent probes. We also tried to demonstrate the monitoring of H_2S in living animal with our probe **3**-PAA-$NaYF_4$:Yb/Mn/Er with red emission. The mice were subcutaneously injected with the probe, Na_2S and saline were then respectively injected to the experimental and control mouse at the same site. Compared with control mice treated with normal saline, the UCL at 650 nm increased significantly after treatment with Na_2S (Figure S35, Supporting Information). These results confirmed the feasibility of monitoring of H_2S in vivo by our probes.

2.5. Practical Application

To evaluate the applicability of the UCL probes in blood samples, blood serum was collected from nude mice. Using a standard addition procedure, the serum spiked with Na_2S and tested in the assay. Response of the **3**-$NaYF_4$:Yb/Er/Mn in diluted mouse serum samples with Na_2S concentrations of 0×10^{-3} to 0.13×10^{-3} M was measured and the UCL intensity displays linear increase with increasing Na_2S concentration (Figure S36, Supporting Information), suggesting that the probes could detect Na_2S without interference from biological environment, and the reaction was completed in 30 s at room temperature. To further demonstrate the applicability of our assay in practical applications, we performed recovery experiments using spiked serum samples with 45×10^{-6}, 65×10^{-6}, 105×10^{-6} M of Na_2S (**Table 1**). We observed an average recovery value of 102.09%, indicating that the probes can be used for the detection of H_2S in real samples. High recovery percentages indicate the high accuracy of our colorimetric assay.

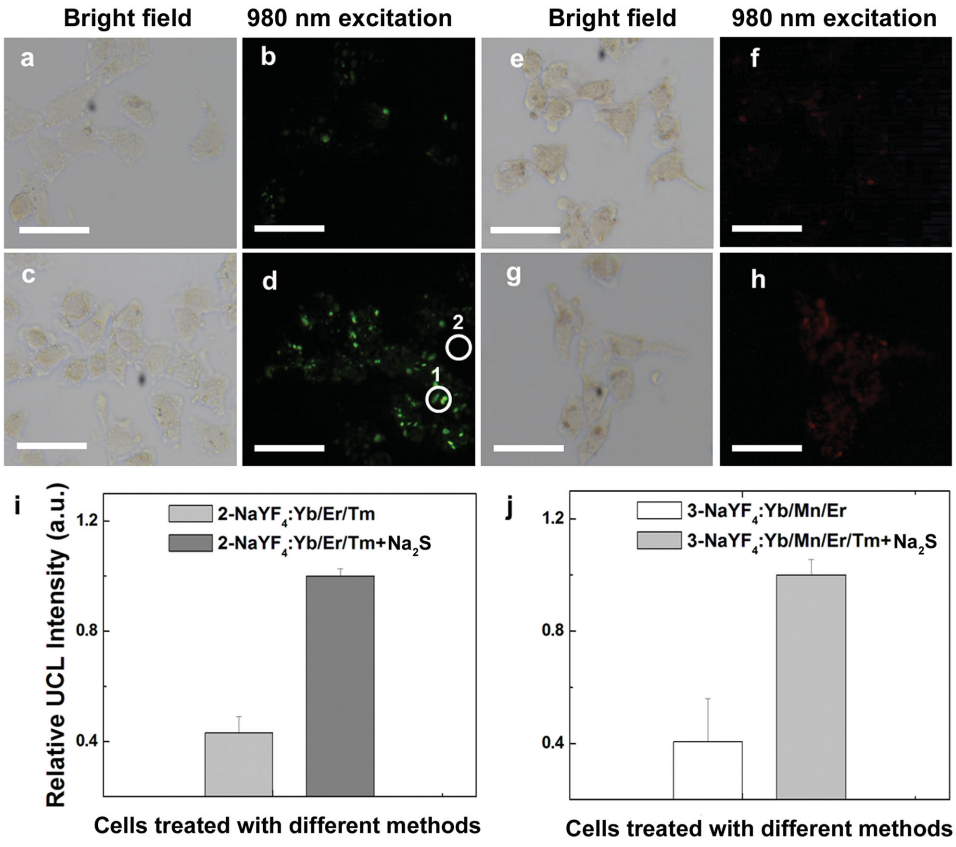

Figure 5. a,b,e,f) Bright-field and UCL images of HeLa cells incubated with **2**-PAA-$NaYF_4$:Yb/Er/Tm (250 μg mL^{-1}), **3**-PAA-$NaYF_4$:Yb/Mn/Er (250 μg mL^{-1}) for 1 h, separately. c,d,g,h) bright-field and UCL images of HeLa cells incubated with **2**-PAA-$NaYF_4$:Yb/Er/Tm (250 μg mL^{-1}), **3**-PAA-$NaYF_4$:Yb/Mn/Er (250 μg mL^{-1}) for 1 h, and then incubated with Na_2S (100×10^{-6} M) for 30 min. Quantification of UCL signals of region 1 and region 2 by Imaging J. The scale bars are 50 μm. i,j) Quantification of the fluorescence signals from a–h) cell imaging. Data were normalized to fluorescence intensity from HeLa cells after treatment with Na_2S. Error bars are ± SD, $n = 3$.

3. Conclusion

In summary, we have developed a new dye-assembled sulfide sensing platform consisting of four nanoprobes: **1**-PAA-$NaYF_4$:Yb/Er/Tm, **2**-PAA-$NaYF_4$:Yb/Er/Tm, **3**-PAA-$NaYF_4$:Yb/Er/Tm, and **3**-$NaYF_4$:Yb/Er/Mn. The powerful strategy that incorporates designed chromophores onto upconversion nanoparticles has created a cascade of probes with emission spectra ranging from visible to NIR. Furthermore, these nanosystems exhibited high sensitivity and fast response to H_2S within 5 s, while refraining from the interference of other thiol species in physiological environments. Taken together the benefits of rapid recognition by chromophores and the intriguing photophysical properties by UCNPs, we successfully demonstrated that our hybrid nanoprobes were also applicable for H_2S detection in live cells and in blood serum. This fast, sensitive, and selective probe has the potential to be a useful tool for disease diagnosis associated with H_2S in further clinical medicine. More importantly, the design strategy could be readily expanded to other analytes with simple tuning of chromophores and nanoparticles.

Table 1. Results of the H_2S recovery experiments performed in diluted serum samples.

Added [$\times 10^{-6}$ M]	Found [$\times 10^{-6}$ M]	Recovery [%]
45	47.76	106.13
65	67.89	104.44
105	100.47	95.69

4. Experimental Section

Materials: $Y(CH_3CO_2)_3 \cdot xH_2O$ (99.9%), $Yb(CH_3CO_2)_3 \cdot 4H_2O$ (99.9%), $Tm(CH_3CO_2)_3 \cdot xH_2O$ (99.9%), $MnCl_2 \cdot 4H_2O$ (99%), NaOH (98+%), NH_4F (98+%), 1-octadecene (90%), and oleic acid (OA) (90%) were purchased from Sigma–Aldrich and used as received without further purification.

Characterization: TEM measurements were carried out on a JEL-1400 transmission electron microscope (JEOL) operating at an acceleration voltage of 100 kV. UV–vis spectra were performed using a fluorimeter and UV/Vis instrument, SpectraMax M2, Molecular Devices. Upconversion luminescence spectra were obtained with a DM150i monochromator equipped with a R928 photon counting photomultiplier tube (PMT), in conjunction with a 980 nm diode laser. Digital photographs were taken with a Nikon D700 camera. Cell imaging was performed on an Olympus BX51 microscope with a xenon lamp adapted to a 980 nm diode laser. The luminescence micrographs were recorded with a Nikon DS-Ri1 color imaging system. Image analysis was performed using NIS-Elements Advanced Research software (Nikon).

Synthesis of $NaYF_4$:Yb/Er/Tm (20/0.16/0.04 mol%) Nanoparticle: To a 50 mL flask containing oleic acid (3 mL) and 1-octadecene (7 mL) was added a water solution (2 mL) containing $Y(CH_3CO_2)_3$ (0.32 mmol), $Yb(CH_3CO_2)_3$ (0.08 mmol), $Er(CH_3CO_2)_3$ (0.00064 mmol) and $Tm(CH_3CO_2)_3$ (0.00016 mmol). The resulting mixture was heated to 150 °C for 1.5 h to form lanthanide oleate complexes and remove water, and then cooled down to room temperature. Subsequently, a methanol solution (6 mL) containing NH_4F (1.6 mmol) and NaOH (1 mmol) was added and stirred at 50 °C for 30 min. The reaction temperature was then increased to 100 °C to remove the methanol from the reaction mixture. Upon removal of the methanol, the solution was heated to 290 °C and maintained at this temperature under an argon flow for 1.5 h, at which time the mixture was cooled down to room temperature. The resulting nanoparticles were precipitated out by the addition of ethanol, collected by centrifugation, washed with ethanol for three times, and finally redispersed in cyclohexane (4 mL).

Synthesis of $NaYF_4$:Yb/Mn/Er (20/30/2 mol%) Nanoparticles: The pure red color Mn^{2+} ions doped $NaYF_4$:Yb/Mn/Er nanocrystals were prepared by reported method.[14b] Typically, $MnCl_2$,(0.6 mL, 0.5 M) $Y(NO_3)_3$ (1.0 mL, 0.5 M), $Yb(NO_3)_3$ (0.9 mL, 0.2 M), and $Er(NO_3)_3$ (0.1 mL, 0.2 M) were added to a mixture of NaOH (0.3 g), deionized water (1.5 mL), oleic acid (5 mL), and ethanol (10 mL) under thorough stirring. Then, deionized water (2 mL) contained NaF (4 mmol) was added dropwise to the mixture. After vigorous stirring at room temperature for 15 min, the colloidal solutions were transferred into a 25 mL Teflon-lined autoclave, sealed, and heated at 200 °C for 8 h. The systems were then allowed to cool to room temperature. The final products were collected by centrifugation, washed with ethanol and deionized water for several times to remove any possible remnants.

Measurement of Quantum Yield: The quantum yield of $NaYF_4$:Yb/Er/Tm and $NaYF_4$:Yb/Mn/Er was measured by reported method.[13] In detail, a barium-sulfate-coated integrating sphere was employed from Edinburgh instruments. The integrating sphere was mounted on the fluorimeter with the entry and output ports of the sphere located in 90° geometry from each other in the plane of the spectrometer. The UCNPs samples were held in a quartz cuvette located in the center of the integrating sphere. Samples were excited with a 980 nm laser diode (Hi-Tech optoelectronics Co., Ltd). All the spectroscopic data collected were corrected for the spectral response of both the fluorimeter and the integrating sphere. The QY is defined as:

$$QY = \frac{\#\text{photons emitted}}{\text{photons absorbed}} = \frac{L_{sample}}{E_{reference} - E_{sample}} \quad (2)$$

where QY is the quantum yield, L_{sample} is the emission intensity, $E_{reference}$ and E_{sample} are the intensities of the excitation light not absorbed by the sample and the reference sample, respectively.

Preparation of Hydrophilic Nanoparticles: The preparation of the water-soluble nanocrystals was firstly performed as reported by Capobianco and co-workers.[16] First, the OA-$NaYF_4$:Yb/Er/Tm and OA-$NaYF_4$:Yb/Mn/Er were washed with hydrochloric acid and obtain water-dispersible, ligand-free, brightly upconverting $NaYF_4$:Yb/Er/Tm and $NaYF_4$:Yb/Mn/Er. Then ligand-free UCNPs were dispersed in the PAA solution (10 mg mL^{-1}, adjusted to pH 7 with NaOH), followed by stirring overnight and PAA–UCNPs were obtained. Finally, the PAA–UCNPs were washed with deionized water by sonication and centrifugation.

Loading Compound **1**, **2,** *and* **3** *to PAA–UCNPs*: compounds **1**, **2,** or **3** (10×10^{-3} M) was dissolved in DMSO and added dropwise into water solution containing PAA-functionalized UCNPs ($NaYF_4$:Yb/Er/Tm and $NaYF_4$:Yb/Mn/Er, 1 mg mL^{-1}), respectively. The solution was then stirred overnight. Free compounds **1**, **2,** and **3** were removed by centrifugation. The precipitate was washed with water by centrifugation. The as-obtained hybrid materials (**1**-PAA-$NaYF_4$:Yb/Er/Tm, **2**-PAA-$NaYF_4$:Yb/Er/Tm, **3**-PAA-$NaYF_4$:Yb/Er/Tm, and **3**-PAA-$NaYF_4$:Yb/Mn/Er) were suspended by a brief sonication to form a homogeneous solution.

Procedures for H_2S Sensing: Stock solutions of the H_2S (12×10^{-3} M) were prepared in H_2O. A stock solution of **1**-PAA-$NaYF_4$:Yb/Er/Tm, **2**-PAA-$NaYF_4$:Yb/Er/Tm, **3**-PAA-$NaYF_4$:Yb/Er/Tm, and **3**-PAA-$NaYF_4$:Yb/Mn/Er (0.25 mg mL^{-1}) were prepared in water solution. The sensing of kinds of as-prepared materials to H_2S was performed by adding different amount of H_2S stock solution to 100 µL solution of **1**-PAA-$NaYF_4$:Yb/Er/Tm, **2**-PAA-$NaYF_4$:Yb/Er/Tm, **3**-PAA-$NaYF_4$:Yb/Er/Tm, and **3**-PAA-$NaYF_4$:Yb/Mn/Er, respectively. Test samples for selectivity experiments were prepared by adding appropriate amounts of other ions, ROS stock solution with a similar procedure, fluorescent spectra of the samples were recorded after incubation for 5 min.

Movie: Real-time color change in response of **1**-PAA-$NaYF_4$:Yb/Er/Tm, **2**-PAA-$NaYF_4$:Yb/Er/Tm, **3**-PAA-$NaYF_4$:Yb/Er/Tm aqueous solution upon addition of H_2S solution and then further addition of excessive H_2SO_4. 3 µL Na_2S aqueous solution (12×10^{-3} M) was added, and the color was changed from red (**1**-PAA-UCNPs), purple (**2**-PAA-UCNPs), and blue (**3**-PAA-UCNPs) to dark yellow within 5 s. After the addition of excessive H_2SO_4 (10×10^{-3} M, 10 µL), the color recovery to red, purple, and blue was completed within 5 s.

Cell Culture: The HeLa cell lines were grown in DMEM medium supplemented with 10% (v/v) fetal bovine serum (FBS) and antibiotics (100 U mL^{-1} antibiotic and 100 mg mL^{-1} antimycotic) in an atmosphere at 37 °C with 5% (v/v) CO_2.

Cytotoxicity of the As-Prepared Nanoprobes: To study the cytotoxicity, 100 µL of cell suspension (≈10 000 cells $well^{-1}$) in a 96-well plate was dispensed. The cells were pre-incubated for 12 h in high glucose media (DMEM) with 10% FBS and 1% Anti–Anti with in a humidified incubator (37 °C, 5% CO_2). Next, different concentrations of UCNPs, **1**-PAA-$NaYF_4$:Yb/Er/Tm, **2**-PAA-$NaYF_4$:Yb/Er/Tm, **3**-PAA-$NaYF_4$:Yb/Er/Tm, and **3**-PAA-$NaYF_4$:Yb/Mn/Er (0, 200, 400, 600, 800, 1000, and 1200 µg mL^{-1}, diluted in DMEM) were then added to the wells, respectively. The cells were subsequently incubated for 24 h at 37 °C under 5% CO_2. Then, MTT (20 µL, 5 mg mL^{-1}) was added to each well, and the plate was incubated for an additional 4 h at 37 °C under 5% CO_2. After the addition of 100 µL DMSO, the assay plate was allowed to stand at room temperature for 2 h. The optical density OD570 value (Abs) of each well, with background subtraction at 690 nm, was measured by means of a fluorimeter and UV–Vis instrument, SpectraMax M2, Molecular Devices. The following formula was used to calculate the inhibition of cell growth:

Cell viability(%) = (mean Abs value of treatment group/mean Abs value of control)×100%

Cell Imaging: HeLa cell lines were maintained at 37 °C in 5% CO_2 in DMEM media, respectively, both supplemented with 10% FBS, 100 U mL^{-1} penicillin and 100 mg mL^{-1} streptomycin. The cells were plated at around 60%–70% confluency 24 h before imaging experiments in 35 mm culture dishes. Prior to imaging experiments, the cancer cells were incubated with **2**-$NaYF_4$:Yb/Er/Tm or **3**-$NaYF_4$:Yb/Mn/Er (250 µg mL^{-1}) for 1 h and then treated cells with Na_2S (0.1×10^{-3} M) solution for 30 min. The cell lines were further washed using cell culture media and subsequently imaged at ambient temperature. The image quantification was obtained by quantitatively analyzing the intensity of the cell imaging before and after treatment with Na_2S with software Imaging J. Data was normalized by the UCL intensity from cell after the addition of Na_2S. Error bars were obtained by measuring the intensities from three individual cells from the image.

Upconversion Luminescence In Vivo Imaging: In vivo upconversion luminescence imaging was performed with modified Maestro in vivo imaging system (CRi Inc) from EINST Technology. In this system, using a 980 nm optical laser (Hi-Tech optoelectronics Co., Ltd) as the excitation source was used as the excitation sources. Images of luminescent signals were analyzed with the MaxIm DL Pro 5 Imaging Software. Male nude mice (4 weeks old, ≈20 g) were subcutaneously injected with **3**-PAA-$NaYF_4$:Yb/Mn/Er (5 mg mL^{-1}, 50 µL) and divided into two groups. The control group was subcutaneously injected with saline, and the experimental group was subcutaneously injected with Na_2S (50 µL, 0.4×10^{-3} M) after injected with nanoparticles. In vivo UCL imaging was detected 10 min after subcutaneously injection of Na_2S. UCL signals were collected at 630 ± 30 nm.

Detection of H_2S Levels in Mice Plasma: Nude mice (≈20 g) were sacrificed and blood was removed by cardiac puncture into heparinized tubes. Then diluted serum (10%, 150 µL × 6) was transferred from each sample into

ultra-micro (200 µL) cuvettes. Na_2S was spiked into each sample to a final concentration of 26.7×10^{-6}, 53.3×10^{-6}, 80×10^{-6}, 106.7×10^{-6}, and 133.3×10^{-6} M, followed by addition of **3**-$NaYF_4$:Yb/Mn/Er (final concentration: 0.25 mg mL^{-1}). Zero point was obtained by trapping sulfide with $ZnCl_2$ (1×10^{-3} M) followed by centrifugation and addition of **3**-$NaYF_4$:Yb/Mn/Er. The UCL intensities were measured on UCL test system.

Supporting Information

Supporting Information is available from the Wiley Online Library or from the author.

Acknowledgements

The authors gratefully acknowledge the A*STAR Joint Council Office (JCO), Singapore (Grant 1231AFG028) for the financial support.

Received: September 2, 2015
Revised: October 13, 2015
Published online: November 30, 2015

[1] Y. Qian, J. Karpus, O. Kabil, S.-Y. Zhang, H.-L. Zhu, R. Banerjee, J. Zhao, C. He, *Nat. Commun.* **2011**, *2*, 495.
[2] D. J. Lefer, *Proc. Natl. Acad. Sci. USA* **2007**, *104*, 17907.
[3] A. Papapetropoulos, A. Pyriochou, Z. Altaany, G. Yang, A. Marazioti, Z. Zhou, M. G. Jeschke, L. K. Branski, D. N. Herndon, R. Wang, C. Szabó, *Proc. Natl. Acad. Sci. USA* **2009**, *106*, 21972.
[4] L. Li, P. K. Moore, *Trends Pharmacol. Sci.* **2008**, *29*, 84.
[5] a) G. Yang, L. Wu, B. Jiang, W. Yang, J. Qi, K. Cao, Q. Meng, A. K. Mustafa, W. Mu, S. Zhang, S. H. Snyder, R. Wang, *Science* **2008**, *322*, 587; b) Y. Pei, B. Wu, Q. Cao, L. Wu, G. Yang, *Toxicol. Appl. Pharmacol.* **2011**, *257*, 420.
[6] P. Kamoun, M.-C. Belardinelli, A. Chabli, K. Lallouchi, B. Chadefaux-Vekemans, *Am. J. Med. Genet. A* **2003**, *116A*, 310.
[7] A. Xuan, D. Long, J. Li, W. Ji, M. Zhang, L. Hong, J. Liu, *J. Neuroinflammation* **2012**, *9*, 202.
[8] S. Fiorucci, E. Antonelli, A. Mencarelli, S. Orlandi, B. Renga, G. Rizzo, E. Distrutti, V. Shah, A. Morelli, *Hepatology* **2005**, *42*, 539.
[9] a) L. Yuan, F. Jin, Z. Zeng, C. Liu, S. Luo, J. Wu, *Chem. Sci.* **2015**, *6*, 2360; b) K. Sasakura, K. Hanaoka, N. Shibuya, Y. Mikami, Y. Kimura, T. Komatsu, T. Ueno, T. Terai, H. Kimura, T. Nagano, *J. Am. Chem. Soc.* **2011**, *133*, 18003; c) H. Peng, Y. Cheng, C. Dai, A. L. King, B. L. Predmore, D. J. Lefer, B. Wang, *Angew. Chem. Int. Ed.* **2011**, *50*, 9672; d) T. S. Bailey, M. D. Pluth, *J. Am. Chem. Soc.* **2013**, *135*, 16697; e) S. S. Nagarkar, T. Saha, A. V. Desai, P. Talukdar, S. K. Ghosh, *Sci. Rep.* **2014**, *4*, 7053; f) P. Zhang, J. Li, B. Li, J. Xu, F. Zeng, J. Lv, S. Wu, *Chem. Commun.* **2015**, *51*, 4414; g) Y. Li, W. Luo, N. Qin, J. Dong, J. Wei, W. Li, S. Feng, J. Chen, J. Xu, A. A. Elzatahry, M. H. Es-Saheb, Y. Deng, D. Zhao, *Angew. Chem. Int. Ed.* **2014**, *53*, 9035; h) L. He, W. Lin, Q. Xu, H. Wei, *Chem. Commun.* **2015**, *51*, 1510; i) Y. Zhou, W. Chen, J. Zhu, W. Pei, C. Wang, L. Huang, C. Yao, Q. Yan, W. Huang, J. S. C. Loo, Q. Zhang, *Small* **2014**, *10*, 4874; j) S. Liu, L. Zhang, T. Yang, H. Yang, K. Y. Zhang, X. Zhao, W. Lv, Q. Yu, X. Zhang, Q. Zhao, X. Liu, W. Huang, *ACS Appl. Mater. Interfaces* **2014**, *6*, 11013; k) Y. Qian, L. Zhang, S. Ding, X. Deng, C. He, X. E. Zheng, H.-L. Zhu, J. Zhao, *Chem. Sci.* **2012**, *3*, 2920.
[10] a) F. Auzel, *Chem. Rev.* **2004**, *104*, 139; b) G. Tian, W. Ren, L. Yan, S. Jian, Z. Gu, L. Zhou, S. Jin, W. Yin, S. Li, Y. Zhao, *Small* **2013**, *9*, 1928; c) N. M. Idris, M. K. Gnanasammandhan, J. Zhang, P. C. Ho, R. Mahendran, Y. Zhang, *Nat. Med.* **2012**, *18*, 1580; d) J. Wang, R. Deng, M. A. MacDonald, B. Chen, J. Yuan, F. Wang, D. Chi, T. S. Andy Hor, P. Zhang, G. Liu, Y. Han, X. Liu, *Nat. Mater.* **2014**, *13*, 157; e) S. Han, R. Deng, X. Xie, X. Liu, *Angew. Chem. Int. Ed.* **2014**, *53*, 11702; f) O. Lehmann, K. Kompe, M. Haase, *J. Am. Chem. Soc.* **2004**, *126*14935; g) J. Shen, G. Chen, A.-M. Vu, W. Fan, O. S. Bilsel, C.-C. Chang, G. Han, *Adv. Opt. Mater.* **2013**, *1*, 644; h) L. Zhao, J. Peng, Q. Huang, C. Li, M. Chen, Y. Sun, Q. Lin, L. Zhu, F. Li, *Adv. Funct. Mater.* **2013**, *24*, 363; i) J. Park, K. J. An, Y. S. Hwang, J. G. Park, H. J. Noh, J. Y. Kim, J. H. Park, N. M. Hwang, T. Hyeon, *Nat. Mater.* **2004**, *3*, 891; j) J. Liu, Y. Liu, W. Bu, J. Bu, Y. Sun, J. Du, J. Shi, *J. Am. Chem. Soc.* **2014**, *136*, 9701; k) F. Zhang, R. C. Haushalter, R. W. Haushalter, Y. F. Shi, Y. C. Zhang, K. L. Ding, D. Y. Zhao, G. D. Stucky, *Small* **2011**, *7*, 1972; l) Y. Min, J. Li, F. Liu, E. K. L. Yeow, B. Xing, *Angew. Chem.* **2014**, *126*, 1030; m) Y. W. Zhang, X. Sun, R. Si, L. P. You, C. H. Yan, *J. Am. Chem. Soc.* **2005**, *127*, 3260; n) R. Deng, F. Qin, R. Chen, W. Huang, M. Hong, X. Liu, *Nat. Nano* **2015**, *10*, 237; o) X. Liu, C.-H. Yan, J. A. Capobianco, *Chem. Soc. Rev.* **2015**, *44*, 1299; p) J. Lai, Y. Zhang, N. Pasquale, K.-B. Lee, *Angew. Chem. Int. Ed.* **2014**, *53*, 14419; q) D. Yang, P. A. Ma, Z. Hou, Z. Cheng, C. Li, J. Lin, *Chem. Soc. Rev.* **2015**, *44*, 1416; r) G. Chen, H. Agren, T. Y. Ohulchanskyy, P. N. Prasad, *Chem. Soc. Rev.* **2015**, *44*, 1680; s) W. Zheng, P. Huang, D. Tu, E. Ma, H. Zhu, X. Chen, *Chem. Soc. Rev.* **2015**, *44*, 1379.
[11] a) H. S. Mader, O. S. Wolfbeis, *Anal. Chem.* **2010**, *82*, 5002; b) D. E. Achatz, R. J. Meier, L. H. Fischer, O. S. Wolfbeis, *Angew. Chem., Int. Ed.* **2010**, 260; c) L. N. Sun, H. S. Peng, M. I. J. Stich, D. Achatz, O. S. Wolfbeis, *Chem. Commun.* **2009**, 5000; d) L. Yao, J. Zhou, J. Liu, W. Feng, F. Li, *Adv. Funct. Mater.* **2012**, *22*, 2667; e) L. Zhao, J. Peng, M. Chen, Y. Liu, L. Yao, W. Feng, F. Li, *ACS Appl. Mater. Interfaces* **2014**, *6*, 11190; f) R. Deng, X. Xie, M. Vendrell, Y.-T. Chang, X. Liu, *J. Am. Chem. Soc.* **2011**, *133*, 20168; g) J. Peng, W. Xu, C. L. Teoh, S. Han, B. Kim, A. Samanta, J. C. Er, L. Wang, L. Yuan, X. Liu, Y.-T. Chang, *J. Am. Chem. Soc.* **2015**, *137*, 2336.
[12] J. Liu, Y.-Q. Sun, J. Zhang, T. Yang, J. Cao, L. Zhang, W. Guo, *Chem. A Eur. J.* **2013**, *19*, 4717.
[13] J. C. Boyer, F. C. J. M. van Veggel, *Nanoscale* **2010**, *2*, 1417.
[14] a) F. Wang, R. R. Deng, J. Wang, Q. X. Wang, Y. Han, H. M. Zhu, X. Y. Chen, X. G. Liu, *Nat. Mater.* **2011**, *10*, 968; b) G. Tian, Z. Gu, L. Zhou, W. Yin, X. Liu, L. Yan, S. Jin, W. Ren, G. Xing, S. Li, Y. Zhao, *Adv. Mater.* **2012**, *24*, 1226.
[15] A. Bednarkiewicz, M. Nyk, M. Samoc, W. Strek, *J. Phys. Chem. C* **2010**, *114*, 17535.
[16] N. Bogdan, F. Vetrone, G. A. Ozin, J. A. Capobianco, *Nano Lett.* **2011**, *11*, 835.